Tertiary Structure of an RNA Pseudoknot Is Stabilized by "Diffuse" Mg^{2+} Ions†

Ana Maria Soto,‡,|| Vinod Misra,§ and David E. Draper*,‡

Department of Chemistry, Johns Hopkins University, Baltimore, Maryland 21218, and Department of Pediatrics and Communicable Disease, University of Michigan, Ann Arbor, Michigan 48109

Received August 17, 2006; Revised Manuscript Received December 23, 2006

ABSTRACT: The aim of this study is to obtain a comprehensive experimental and theoretical description of the contributions of Mg^{2+} ions to the free energy of folding a pseudoknot RNA tertiary structure. A fluorescence method for measuring the effective concentration of Mg^{2+} in the presence of an RNA was used to study Mg^{2+}−RNA interactions with both folded and partially unfolded forms of an RNA pseudoknot. These data established the excess number of Mg^{2+} ions accumulated by the folded or partially unfolded RNAs as a function of bulk Mg^{2+} concentration, from which free energies of Mg^{2+}−RNA interactions were derived. Complementary thermal melting experiments were also used to obtain RNA-folding free energies. These experimental data were compared with the results of calculations based on the nonlinear Poisson−Boltzmann equation, which describes the interaction of "diffuse" (fully hydrated) Mg^{2+} ions with the different RNA forms. Good agreement between the calculations and experimental data suggests that essentially all of the Mg^{2+}-induced stabilization of the native pseudoknot structure arises from the stronger interaction of diffuse ions with the folded tertiary structure compared to that with a partially unfolded state. It is unlikely that the stability of the RNA depends on dehydrated ions bound to specific sets of RNA ligands in the folded state. The data also suggest that the Mg^{2+}-dependent free energy of folding is sensitive to factors that influence the ensemble of RNA conformations present in the partially unfolded state.

Many RNAs fold into compact structures (*1*, *2*) that are required for biological functions (*3*, *4*). The close approach of negatively charged phosphate groups in such RNAs is associated with a large electrostatic free energy opposed to folding. Because ions may reduce the repulsive energies between RNA phosphates, the concentrations and types of salt present in solution strongly affect the stability of folded RNAs (*5*, *6*) and modulate protein interactions and other molecular processes involving RNA. Mg^{2+} and other divalent cations are particularly effective at stabilizing RNA tertiary structure (*7*, *8*); however, the mechanisms by which they stabilize RNA are still being elucidated. Early work, especially with tRNA, postulated that folded RNAs are primarily stabilized by Mg^{2+} coordinated to specific RNA ligands (*9*). However, more recent electrostatic models based on the Poisson−Boltzmann (PB[1]) theory of ion−RNA interactions suggest that much of the work of stabilizing RNA structures is done by "diffuse" (fully hydrated) Mg^{2+} ions that interact with the RNA electrostatic field but are not bound to specific sites (*10*, *11*).

Currently, only a few experimental sets of data, obtained under a limited range of experimental conditions, can be compared directly with calculations based on theoretical models of Mg^{2+}−RNA interactions (*8*, *10*, *12*). The objective of the present study is to obtain a comprehensive experimental description of the Mg^{2+}-dependent folding of an RNA tertiary structure in terms of thermodynamic parameters that can be compared to calculations based on the Poisson−Boltzmann theory. The RNA chosen for this study is an RNA pseudoknot from beet western yellow virus (BWYV1) (Figure 1A), which has several advantages for our analysis: it has a stable tertiary structure in the absence of Mg^{2+} so that Mg^{2+} interaction free energies can be directly measured; it has well-defined unfolded intermediate states, allowing for theoretical and experimental evaluation of specific transitions; and its high-resolution crystal structure is known (*13*, *14*), making detailed theoretical calculations possible.

A comparison of our experimental data to calculations based on the Poisson−Boltzmann model suggests that essentially all of the Mg^{2+}-induced stabilization of the native pseudoknot structure arises from the stronger interaction of diffuse ions with the folded tertiary structure compared to that with a partially unfolded state. Importantly, we do not need to invoke site-bound ions to understand the ion dependence of BWYV RNA folding. In this regard, our calculations delineate the important features of ion−RNA interactions that must be taken into account if the mechanisms by which Mg^{2+} ions stabilize RNA are to be quantitatively understood.

† This work was supported by NIH grant RO1 GM58545. A.M.S. was partially supported by the Burroughs Wellcome Fund.

* To whom correspondence should be addressed. Tel: (410) 235-3245. Fax: (410) 516-8420. E-mail: draper@jhu.edu.

‡ Johns Hopkins University.

§ University of Michigan.

|| Present address: Department of Chemistry, The College of New Jersey, Ewing, New Jersey 08628-0718.

[1] Abbreviations: BWYV, beet western yellow virus; HQS, 8-hydroxy quinoline 5-sulfonic acid; PB, Poisson−Botlzman; NLPB, non-linear Poisson−Boltzmann.

10.1021/bi0616753 CCC: $37.00
Published on Web 02/23/2007

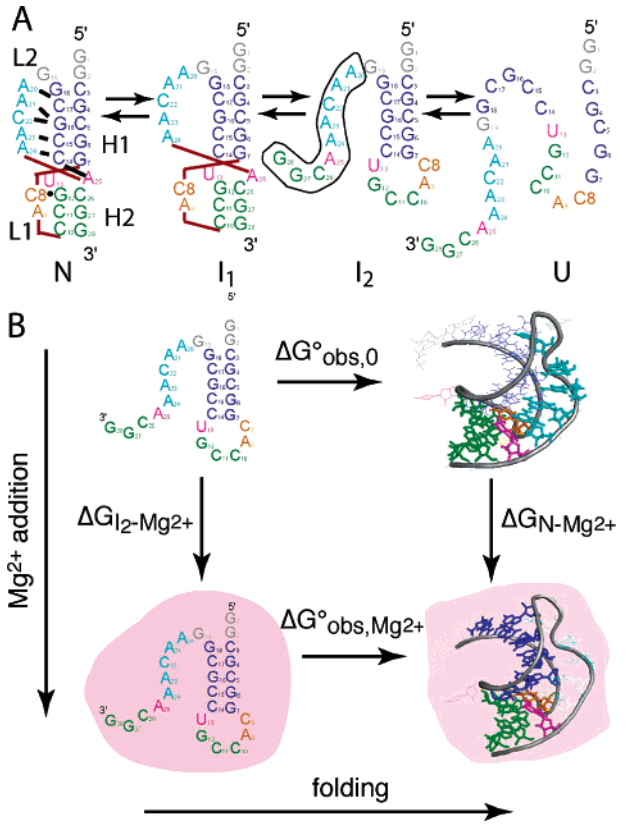

FIGURE 1: Folding of the BWYV pseudoknot RNA. (A) Unfolding of BWYV RNA in three two-state transitions, as proposed by Nixon and Giedroc (*29*). The green and dark blue nucleotides form Watson−Crick pairs in the N and I_1 states; only H1 (dark blue helix) forms in the I_2 state. The N state has additional hydrogen bonding, indicated by heavy black lines (*13*). The red lines indicate backbone connectivity. The nine 3′-terminal nucleotides boxed in the I_2 state schematic were changed to U to make U-tail RNA, a mimic of I_2 state RNA. (B) Thermodynamic cycle separating the free energy of RNA tertiary folding from the free energies of Mg^{2+}−RNA interactions, with definitions of folding free energies (horizontal arrows) and Mg^{2+}−RNA interaction free energies (vertical arrows). The pink background in the lower two RNAs indicates the presence of Mg^{2+} in the buffer.

MATERIALS AND METHODS

RNAs and Buffers. RNAs were produced by *in vitro* transcription from synthetic, double-stranded DNA utilizing T7 RNA polymerase (*15*). Mixtures containing 17 nM DNA template (45 base pairs, for the 17 base-pair T7 promoter and 28 nt transcript), 20 mM $MgCl_2$, 40 mM Tris-HCl at pH 8.1, 80 mg/mL PEG 8000, 4 mM each of ATP, GTP, UTP, and CTP, 1 mM spermidine, 10 mM DTT, 0.01% Triton X100, and ~0.4 mg/mL T7 RNA polymerase were incubated at 37 °C for 10 h. Polymerase with a 6-histidine tag was purified as described (*16*). The resulting RNAs were purified by preparative denaturing gel electrophoresis, excision of the desired product, and electroelution of the RNA using an Elutrap Electrophoresis Chamber (Schleicher & Schuell). The purified RNAs were equilibrated at the desired conditions by filtration using Centricon YM 3000 filters; 125 mM EDTA was included in the first wash. The concentration of each RNA solution was determined at 260 nm and 95 °C using the following molar extinction coefficients (mM^{-1} cm^{-1}) in the following strands: BWYV RNA, 261.1; U-tail RNA, 256.1. These values were calculated by extrapolation of the tabulated values of the dinucleotides and monomer bases at 25 °C to high temperatures, using procedures reported earlier (*17*, *18*).

Buffers contained 10 mM MOPS at pH 7.0, made by adjusting the acid form of the buffer to the desired pH with NaOH; thus, the buffer contributes 4 mM Na^+ to the overall cation concentration. NaCl was added as necessary. The total Na^+ concentration present in an experiment (MOPS buffer plus NaCl) is specified in the text and Figure legends. The pH dependence of melting transitions was measured using buffers with pK_a values within 1 pH unit of the desired pH (MES, MOPS, HEPES, and EPPS). Mg^{2+} was always added as the chloride salt. MOPS, NaCl, MgCl2, NTPs, and other chemicals were purchased from Sigma and used without further purification. 8-Hydroxyquinoline 5-sulfonic acid (HQS) was purchased from Sigma and recrystallized two times to improve its purity (*19*).

UV and Fluorescence Experiments. Absorbance versus temperature profiles (melting curves) for each RNA were measured at 260 and 280 nm with a thermoelectrically controlled Varian Cary Bio400 spectrophotometer. The temperature was scanned at a heating rate of 0.5 °C/min. Both BWYV and U-tail RNAs were found to reversibly unfold at this heating rate. Melting temperatures (T_M) and van't Hoff enthalpies ($\Delta H°$) for each of the three unfolding transitions were extracted from the data using the program Global Melt Fit as described (*20*). Free energies of unfolding were extrapolated to 25 °C using the equation $\Delta G° = \Delta H°(1 - 298/T_M)$.

Determinations of the excess Mg^{2+} accumulated by an RNA were carried out in an Aviv ATF fluorimeter equipped with sample and reference cell compartments, using the fluorescent dye HQS to detect the effective concentration of the Mg^{2+} ion. Representative titration data and a detailed description of the experimental protocol and data analysis are in refs 19 and 21 (*19*, *21*). In brief, reference and sample cuvettes are prepared with identical buffered solutions of the dye and monovalent salt; RNA equilibrated with the same solution is added to the sample cuvette. The cuvettes are titrated with $MgCl_2$. More $MgCl_2$ must be added to the sample cuvette to reach the same fluorescence level (indicative of the effective Mg^{2+} concentration) because of interactions between Mg^{2+} and the RNA. The excess Mg^{2+} is as follows

$$\Delta C_{2+}^{RNA} = \frac{C_{Mg^{2+},sample} - C_{Mg^{2+},ref}}{C_{RNA}} \quad (1)$$

where $C_{Mg^{2+},sample}$ and $C_{Mg^{2+},ref}$ are the total molar concentrations of Mg^{2+} in the sample and reference cuvettes, respectively, and C_{RNA} is the concentration of RNA expressed in terms of either nucleotides or RNA molecules. $C_{Mg^{2+},ref}$ is equivalent to the "bulk" Mg^{2+} ion concentration; we refer to this quantity using the shorthand notation C_{2+}.

The free energy of Mg^{2+} interaction with an RNA was calculated from the area under a plot of ΔC_{2+}^{RNA} versus $\ln(C_{2+})$,

$$\Delta G_{RNA-Mg^{2+}} \cong -RT \int_0^{C_{2+}} \Delta C_{2+}^{RNA} d \ln C_{2+} \quad (2)$$

as derived elsewhere (*21*). To carry out the integration, data were fit to a polynomial, which asymptotically approaches the abcissa at low values of $\ln(C_{2+})$, $y = b(x - a)^2 + c(x -$

$a)^3 + d(x - a)^4$. Higher order terms did not improve the fit of the polynomial to the data. Errors in the calculated ΔG arise because the portion of the ΔC_{2+}^{RNA} curve between $\Delta C_{2+}^{RNA} = 0$ and the first data points, $\Delta C_{2+}^{RNA} \approx 0.01$ ions/nucleotide, must be extrapolated. Trials in which the Γ_{2+} curves calculated from the NLPB equation were truncated at various values of Γ_{2+} and integrated using the above polynomial-fitting procedure suggest, for the data sets presented here, that the magnitude of ΔG is underestimated for integrations that extend to ΔC_{2+}^{RNA} values of ~0.04. However, these errors approximately cancel when $\Delta\Delta G_{Mg^{2+}}$ is calculated from the difference between the integrated ΔC_{2+}^{RNA} curves for N and I state RNAs.

The intrinsic pK_a of a protonated base in the BWYV RNA was estimated from the dependence of the unfolding T_M on pH, as derived from standard linkage analysis (*22*)

$$\frac{1}{T_M} = \frac{1}{T_{M0}} - \frac{R}{\Delta H}\left(\ln\left(1 + \frac{[H^+]}{K_N}\right) - \ln\left(1 + \frac{[H^+]}{K_{I_1}}\right)\right) \quad (3)$$

where T_M is the melting temperature at a given pH, T_{M0} is the melting temperature of the unprotonated pseudoknot, R is the gas constant, ΔH is the enthalpy of of the unfolding transition, and K_N and K_{I_1} are the proton dissociation constants for the folded and first partially unfolded states of the RNA, respectively.

Structural Models and NLPB Calculations. Electrostatic calculations were performed by solving the nonlinear Poisson−Boltzmann equation as described (*10*) using a modified version of the program Delphi (*10*, *23*, *24*). In these calculations, the RNA is modeled by its three-dimensional atomic resolution structure. For the native state, N, the structure was obtained from the atomic coordinates deposited in the Protein Data Bank (access code 437D). The intermediate state, I_2 (Figure 1A), was modeled using the Biopolymer module of the Insight II 97.0 software package (Molecular Simulations Inc., San Diego). It was initially modeled as a hairpin (Helix 1) attached to a 3′ single strand in A-form geometry. By rotation of three bond angles within the single-stranded region, the tail was moved to extreme positions relative to the helix. The resulting models, U-tail Near and U-tail Far, positioned the phosphate of the last nucleotide (G28) either 20.3 or 33.8 Å from the first stem phosphate (G3), respectively. Protons were added to the crystallographic coordinates of each structure using the Biopolymer module of the Insight II. The partial charges for the atoms were derived from the AMBER force field potential (*25*). The partial charges of C8 were assigned by redistributing the charge density of an unprotonated cytosine following the shifts observed in the analysis performed by Pack and coworkers (*26*).

The parameters used in the Qnifft program were macromolecule dielectric constant, 2; solvent dielectric constant, 80; water probe radius, 1.4 Å; and ion exclusion radius, 2.0 Å. A focusing procedure was used to calculate the potentials as described (*10*), with the RNA positioned in a 65 × 65 × 65 cubic lattice. In the initial calculations, the RNA filled 15% of the lattice, approximately 0.2 grids per Å. The resolution was increased in two steps so that in the last calculation, the molecule filled ~90% of the lattice, approximately 1.5 grids per Å. The integral to calculate the excess Mg^{2+} was evaluated as a summation over discrete lattice points as described (*10*, *27*). Electrostatic potentials were iterated to a convergence of less than 10^{-4} kT/e. The results presented here varied by less than 1% for focusing procedures where charge neutrality was maintained to within 2%.

BACKGROUND AND THEORY

In this section, we present a conceptual framework describing the relationship between ion interactions and the folding of an RNA tertiary structure (*21*, *28*), with particular reference to the BWYV RNA pseudoknot shown in Figure 1A. The fully folded, native structure (N state) of this RNA is composed of two Watson−Crick helices (H1 and H2) connected by loops (L1 and L2). The tertiary structure is stabilized by extensive non-canonical hydrogen bonds between the adenines in loop 2 and the minor groove of Helix 1 and by a four-base hydrogen-bonded interaction between the first G−C pair of Helix 2, A25, and C8 (*13*, *14*). Using spectroscopic and calorimetric methods, Nixon and Giedroc (*29*) characterized the equilibrium unfolding pathway of BWYV RNA as three consecutive two-state transitions. An initial loss of a non-canonical hydrogen-bonding network (N → I_1) is followed by the unfolding of Helix 2 (I_1 → I_2) and finally the disruption of Helix 1 (I_2 → U). We consider the reaction from the native RNA (N) to the hairpin intermediate (I_2) as a model of a typical RNA-folding equilibrium between the tertiary structure and a partially unfolded intermediate containing only the secondary structure. For the purposes of our analysis, the I_2 state is modeled by a variant sequence (designated "U-tail" RNA) in which base substitutions in the nine 3′-terminal nucleotides abolish the formation of critical tertiary contacts (the substituted nucleotides are boxed in Figure 1A).

In this article, we experimentally and theoretically evaluate the thermodynamic cycle presented in Figure 1B to determine the contribution of Mg^{2+} to the stability of the N state. For our purposes, this cycle occurs in a solution containing a fixed concentration of monovalent cations. Under these conditions, the N and I_2 states are stable in the absence of Mg^{2+} ((*29*); Results), making it possible to directly measure the Mg^{2+} interaction free energies (vertical arrows, corresponding to $\Delta G_{N-Mg^{2+}}$ and $\Delta G_{I_2-Mg^{2+}}$) using described fluorescence methods (see Materials and Methods). The free energies of RNA folding in the absence or presence of Mg^{2+} (horizontal arrows, corresponding to $\Delta G°_{obs,0}$ and $\Delta G°_{obs,Mg^{2+}}$) can be measured by thermal denaturation experiments. In this cycle, the stabilization of the N state relative to the I_2 state by the addition of $MgCl_2$, $\Delta\Delta G_{Mg^{2+}}$, corresponds to either of two differences:

$$\Delta\Delta G_{Mg^{2+}} = \Delta G°_{obs,Mg^{2+}} - \Delta G°_{obs,0} = \Delta G_{N-Mg^{2+}} - \Delta G_{I_2-Mg^{2+}} \quad (4)$$

Both of these differences can be evaluated experimentally in this system (*21*); the second difference can be calculated from theory.

The Mg^{2+}−RNA interaction free energies defined in Figure 1B are experimentally obtained from measurements of the quantity Γ_{2+}^{RNA}, sometimes called an ion interaction

coefficient (*30*). Though similar quantities have been used in theoretical descriptions of Mg^{2+}−nucleic acid interactions (*31*, *32*), their use in experimental RNA-folding studies is less common. For this reason, the definition of Γ_{2+}^{RNA} and its physical significance are briefly summarized here. Further details are available in ref 21 (*21*).

In a four component system consisting of water, the monovalent salt of RNA, 1:1 salt (e.g., NaCl), and a 2:1 salt (e.g., $MgCl_2$), Γ_{2+}^{RNA} is defined as follows.

$$\Gamma_{2+}^{RNA} \equiv \lim_{m_{RNA}\to 0}\left(\frac{m_{2+}^{RNA} - m_{2+}^{bulk}}{m_{RNA}}\right)_{T,P,\mu_4,m_3} = \left(\frac{\partial m_{2+}}{\partial m_{RNA}}\right)_{T,P,\mu_4,m_3} \quad (5)$$

The temperature (T), pressure (P), chemical potential of the neutral 2:1 salt (μ_4), and the concentration of monovalent salt (m_3) are held constant. The quantity m_{2+} is the molal concentration of Mg^{2+}; m_{2+}^{RNA} refers to the Mg^{2+} concentration in a solution containing RNA, and m_{2+}^{bulk} is the Mg^{2+} concentration that would be found in a similar solution with the same $MgCl_2$ chemical potential (μ_4) but no RNA. Extrapolation to infinitely dilute RNA concentrations ($m_{RNA} \rightarrow 0$) is needed to eliminate the nonideality introduced by finite RNA concentrations. Under these conditions, m_{2+}^{bulk} can be thought of as the Mg^{2+} concentration found an infinite distance away from any RNA molecule. Although Γ_{2+}^{RNA} is defined in terms of molal quantities, the solutions used in this work are sufficiently dilute that molality and molarity concentration units are interchangeable.

Γ_{2+}^{RNA} is the "excess" number of Mg^{2+} ions per RNA molecule, as calculated by comparing the number of ions in solutions with or without RNA present but having the same $MgCl_2$ activity. As previously shown, Γ_{2+}^{RNA} is directly related to the total free energy of Mg^{2+} ion interactions with an RNA, and no assumptions about the kinds of interactions taking place between Mg^{2+} and the RNA are needed to extract Γ_{2+}^{RNA} from experimental data (*21*). Γ_{2+}^{RNA} can also be derived from theoretical calculations and simulations (*23*, *33*), which makes it a useful quantity for comparisons of theory and experiment.

The experimentally measured quantity is ΔC_{2+}^{RNA}, the excess Mg^{2+} per RNA nucleotide when the molar bulk Mg^{2+} concentration is C_{2+} (eq 1, Materials and Methods). ΔC_{2+}^{RNA} is identical to the ion interaction coefficient Γ_{2+}^{RNA}, and C_{2+} corresponds to m_{2+} if (i) there is a sufficient excess of 1:1 salt present, and (ii) the dependence of ΔC_{2+}^{RNA} on RNA concentration is negligible. Both of these conditions are satisfied by the experiments reported here. We refer to both Γ_{2+}^{RNA} and ΔC_{2+}^{RNA} as the excess Mg^{2+} per RNA nucleotide, with RNA specified as N, I_2, or U-tail to indicate the specific RNA or conformational state being reported.

RESULTS

Unfolding of BWYV and U-Tail RNAs. The melting profiles of BWYV RNA at 260 and 280 nm, shown in Figure 2A, define a minimum of three unfolding transitions characterized by 260:280 absorbance ratios of approximately 1:0, 1:1, and 1:2. A least-squares best fit of such transitions to the data, obtained by a standard procedure (*20*), is shown. Detailed studies carried out in solutions containing 500 mM KCl have

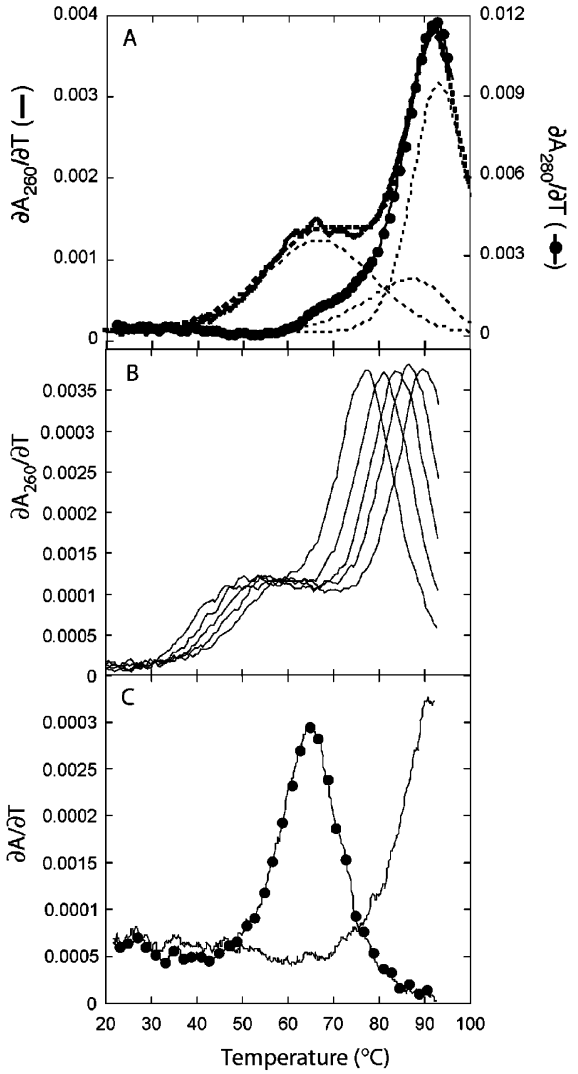

FIGURE 2: UV melting profile of RNAs. (A) Thermal denaturation of BWYV RNA (10 mM sodium MOPS buffer at pH 7.0 and 500 mM NaCl). Data are shown at 260 nm (solid line) or 280 nM (solid line with dots). Three unfolding transitions were globally fit to both sets of data; only the 260 nm curves are shown (dashed lines). (B) BWYV RNA unfolding at different NaCl concentrations (10 mM sodium MOPS buffer at pH 7.0, with 20, 36,70, 116, and 200 mM NaCl). (C) U-tail RNA unfolding at 504 (line) and 4 mM Na^+ (line with dots).

shown that these three apparent transitions are each two-state equilibria between the states of the sequential unfolding pathway shown in Figure 1A (*29*). We find that similar behavior extends to Na^+ concentrations as low as 24 mM (Figure 2B). Thermodynamic parameters from the analysis of these data are summarized in Table 1. The enthalpy changes are approximately independent of salt concentration and in good agreement with the values reported by Nixon and Giedroc (*29*). The T_M values are somewhat larger than those found by these workers at the same pH and monovalent salt concentration, possibly because of the different cations (Na^+ vs K^+) used in the two sets of experiments. The persistence of three distinguishable transitions, with enthalpies that are constant over the entire range of salt concentrations tested, suggests that BWYV RNA folds into a stable pseudoknot at Na^+ concentrations as low as 24 mM at pH 7.0 at 25 °C.

Table 1: Thermodynamic Profiles for the Unfolding of BWYV and U-Tail RNAs[a]

RNA	[Na+] (mM)	T_M1 (°C)	$\Delta H1$ (kcal/mol)	T_M2 (°C)	$\Delta H2$ (kcal/mol)	T_M3 (°C)	$\Delta H3$ (kcal/mol)
BWYV RNA	24	47.4	30	62.5	29	77.2	53
	40	48.1	40	63.3	36	81.3	56
	74	51.2	38	66.9	33	84.4	57
	120	57.2	29	76.1	23	86.2	54
	204	59.4	30	83.7	25	89.1	56
	504	66.7	28	85.9	31	92.0	56
	500[b]	57.5 ± 0.5	32 ± 7	74 ± 2	29 ± 2	90.8 ± 0.5	52.7 ± 0.2
	500[c]	56.4 ± 0.4	29.0 ± 0.5	69.4 ± 0.3	35.4 ± 0.4	91.2 ± 0.1	55.9 ± 0.2
U-Tail RNA	4					65.3	50
	504					94.0	50

[a] All experiments were conducted in 10 mM MOPS buffer at pH 7.0, adjusted to the desired Na^+ concentration with NaCl and using RNA concentrations of ~1.8 μM. The T_M and ΔH values were obtained by simultaneously fitting the first derivatives of the UV melting curves at 260 and 280 nm as described (*20*). The T_M values are accurate to within 0.5 °C and ΔH to within 15%. The ΔH values averaged over all Na^+ concentrations are 33 ± 5 kcal/mol (transition 1), 30 ± 5 kcal/mol (transition 2), and 55 ± 2 kcal/mol (transition 3); these values are the same, within error, as reported elsewhere (*29*). [b] The values are as reported by ref 29 (*29*) from an analysis of UV melting curves but with K^+ as the cation. [c] The values are as reported by ref 29 (*29*) from an analysis of scanning calorimetry data but with K^+ as the cation.

UV melting curves corresponding to the unfolding of U-tail RNA at 4 and 504 mM Na^+ are shown in Figure 2C. Each curve is fit by one transition with an unfolding enthalpy similar to that observed in the unfolding of Helix 1 in BWYV RNA, whereas the T_M values of these transitions are consistent with the Na^+ concentrations used in each experiment (Table 1). The results confirm that the sequence chosen for U-tail RNA forms a structure that corresponds to the second intermediate in BWYV RNA unfolding, that is, a hairpin composed of Helix 1 with a dangling 5′-end. Other mutant sequences designed to disrupt only the interactions between Loop 2 and Helix 1 or the G12-C26-C8 base triplet also resulted in the unfolding of both the tertiary structure and Helix 2 ((*29*), and data not shown).

Effect of Mg^{2+} in BWYV RNA Unfolding. We have used thermal denaturation experiments to monitor BWYV RNA unfolding equilibria as a function of Mg^{2+} concentration (the horizontal arrows in Figure 1B). Figure 3A shows UV melting profiles of BWYV at different Mg^{2+} concentrations. As expected, the T_M of each transition increases with Mg^{2+} concentration. Because BWYV unfolds in two-state transitions, the van't Hoff enthalpies determined from the UV melting profiles can be rigorously used in calculating $\Delta G°_{obs,Mg^{2+}}$ for individual transitions at a reference temperature. These calculated free energies (at 25 °C) are plotted in Figure 3B.

The increase in the number of excess Mg^{2+} ions associated with the RNA upon folding the pseudoknot is calculated from the Wyman linkage relationship (*34*)

$$\left(\frac{1}{RT}\right)\left(\frac{\partial \Delta G°_{obs,Mg^{2+}}}{\partial \ln C_{2+}}\right)_{m_2,m_3} \approx \Gamma^{N}_{2+} - \Gamma^{I_2}_{2+} = \Gamma^{I_2 \rightarrow N}_{2+} \quad (6)$$

where C_{2+} is the bulk Mg^{2+} ion concentration in molar units. This equation is valid when the concentration of NaCl is at least 30-fold higher than that of $MgCl_2$. Under these conditions, the variation of the Mg^{2+} ion activity coefficient with $MgCl_2$ concentration can be neglected (*21*). Thus, $\Delta\Gamma^{trans}_{2+}$, where trans is the particular unfolding transition ($N \rightarrow I_1$, $I_1 \rightarrow I_2$, or $I_2 \rightarrow U$), can be determined from the slopes of the fitted lines in Figure 3B. The experimentally determined slopes for the first and second transitions are −0.341 and −0.388, respectively. $\Delta\Gamma^{I_2 \rightarrow N}_{2+}$ is, therefore, ~0.73 Mg^{2+} ions per RNA, in the range of Mg^{2+} concentrations used in these experiments. This number is compared with calculated values in a subsequent section. (The sum of the free energies of the first two transitions, extracted from the same set of melting curves, has been previously published (*21*).)

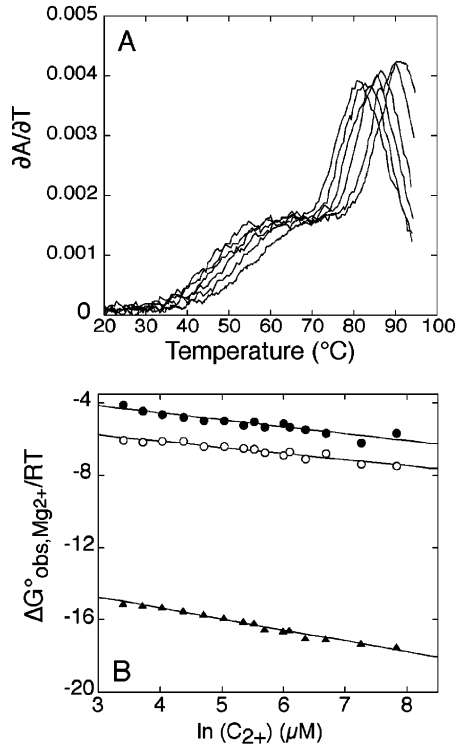

FIGURE 3: Mg^{2+} dependence of BWYV RNA unfolding transitions. (A) Melting profiles in increasing Mg^{2+}concentrations (selected concentrations between 30 μM and 2.51 mM) and constant 54 mM Na^+ and 10 mM MOPS at pH 7.0. (B) Calculated unfolding free energies for three transitions at various Mg^{2+}, as calculated from the melting profiles in panel A and other similar experiments: (●), $N \rightarrow I_1$ transition, slope = −0.388; (○), $I_1 \rightarrow I_2$ transition, slope = −0.341; (▲), $I_2 \rightarrow U$ transition, slope = −0.607.

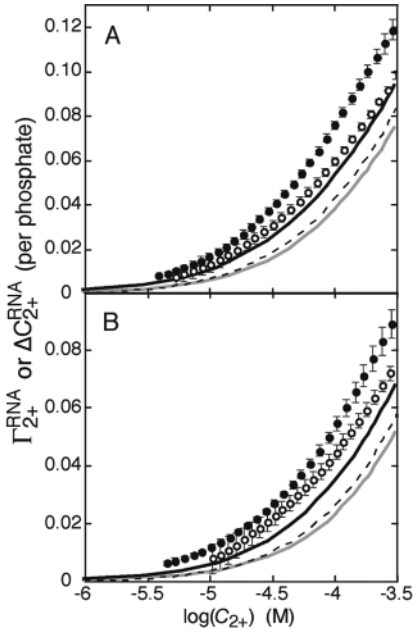

FIGURE 4: Excess Mg^{2+} associated with BWYV and U-tail RNAs at 25 °C and different Na^+ concentrations. Standard buffer (10 mM MOPS at pH 7.0) was used with a total of (A) 54 mM and (B) 79 mM Na^+. The error bars are shown from the average of three independent titrations. The lines are calculations of Γ_{2+}^{RNA} under the same ionic conditions for BWYV RNA (solid black), the U-tail Near RNA model (dashed black), and the U-tail Far RNA model (solid gray).

We used a method based on a fluorescent chelator (see Materials and Methods) to obtain Mg^{2+}−RNA interaction free energies (the vertical arrows in Figure 1B). The results of these measurements, the excess Mg^{2+} per RNA or ΔC_{2+}^{RNA}, are shown in Figure 4 for the native BWYV RNA (N) and the I_2 state mimic, U-tail RNA. BWYV RNA accumulates a larger number of excess ions than does U-tail RNA, as expected from the stabilization of folded BWYV RNA relative to the I_2 state by Mg^{2+}, and the higher Na^+ concentration reduces ΔC_{2+}^{RNA} for either RNA. The ion−RNA interaction free energies obtained by the integration of these data (eq 2, Materials and Methods) are presented in comparison with the theoretical calculations below.

Effect of pH on BWYV RNA Folding. For our calculations, the protonation state of ionizable groups on the RNA was estimated using a set of pH titrations. In particular, the strong pH dependence of the stability of BWYV RNA and the unusual position of C8 against A25 and the major groove edge of the G26−C12 base pair has led to the suggestion that N3 of C8 is protonated and forms a H bond with the O6 of G12 (*13*, *29*). This four-base interaction probably stabilizes Helix 2. In Figure 5, $1/T_M$ (first unfolding transition) is plotted as a function of pH at two different concentrations of Na^+. The data are fitted to an equation in which the protonation constant for the native state, pK_N, and an apparent constant for the first unfolded state, pK_{I_1}, are variables (see Materials and Methods), yielding p$K_N \approx 8.2$ and p$K_{I_1} \approx 6.6$ when the Na^+ concentration is either 79 or 504 mM Na^+. pK_{I_1} is an apparent constant because it does not take into account the multiple A and C protonation sites in the partially unfolded states; protonation of these bases will favor destabilization of the tertiary structure when the pH is lower than ~6. The actual pK_a of C8 in the I1 state is undoubtedly less than 6.6 (compare simulated RNA stability vs pH curves in ref 35 (*35*)). Similar analysis of BWYV RNA pH-dependence data taken from ref 29 (*29*) gave a p$K_N \approx 7.6$. Those data were obtained in the presence of 500 mM K^+; the different monovalent cation may account for the somewhat lower pK_N than that derived from Figure 5 data. The important conclusion is that >90% of the folded RNAs are protonated at the pH of 7.0 used in our experiments. Thus, the structural model of BWYV used for calculations (see next section) contains a protonated cytosine at position 8.

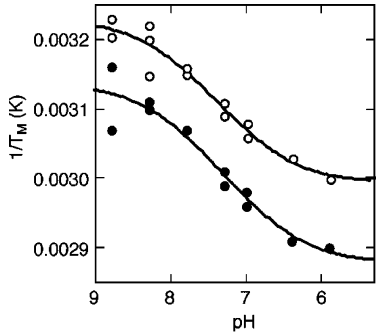

FIGURE 5: pH dependence of BWYV RNA folding. $1/T_m$ of the first unfolding transition is plotted as a function of pH at two Na^+ concentrations. All experiments were conducted in 10 mM buffer (see Materials and Methods) with an additional 75 mM NaCl (○) or 500 mM NaCl (●). The lines are least-square best fits of eq 3 (Materials and Methods). The pK_a values obtained from these fits for the N and I_1 states are 8.2 and 6.6 (75 mM NaCl) or 8.1 and 6.5 (500 mM NaCl), respectively.

Theoretical Calculations of Mg^{2+}−RNA Interactions. We use the nonlinear Poisson−Boltzmann (NLPB) equation to calculate both Γ_{2+}^{RNA} and the electrostatic free energy of Mg^{2+}−RNA interactions (*24*, *36*). The panels in Figure 4 show plots of Γ_{2+}^{N} as a function of log(C_{2+}), calculated using the NLPB equation. Calculations were conducted at the same temperature (25 °C) and monovalent ion concentrations as those of the experiments measuring ΔC_{2+}^{RNA}. In both panels, the calculated values of Γ_{2+}^{N} are less than the ΔC_{2+}^{N} measurements at any value of C_{2+}, though the calculated and measured curves tend to parallel each other.

To carry out similar calculations on the I_2 state mimic, U-tail RNA, we first had to model its structure. The single-stranded RNA of the 3′ tail is expected to be flexible and adopt an ensemble of conformations whose distribution of structures depends on temperature and salt concentrations (*37*−*39*). Rather than attempt to devise a set of models duplicating this ensemble of conformations, we adopted the strategy of preparing two models in which the 3′ tail occupies extreme positions relative to the helix, U-tail Near and U-tail Far (see Materials and Methods). The electrostatic properties of these two models should bracket the average properties of the ensemble. Plots of $\Gamma_{2+}^{I_2}$ as a function of log(C_{2+}), calculated using the NLPB equation in the same way as for Γ_{2+}^{N}, are also shown in Figure 4. NLPB-based calculations of $\Gamma_{2+}^{I_2}$ for these the two extreme models of the partially folded state are shown in Figure 4. The more extended 3′ tail nucleotides are associated with lower values of $\Gamma_{2+}^{I_2}$, in accord with the expectation that RNAs with lower charge density accumulate fewer excess cations (*40*). As with Γ_{2+}^{N}, the calculated $\Gamma_{2+}^{I_2}$ curves all underestimate the number of excess Mg^{2+} ions when compared with the experimental data.

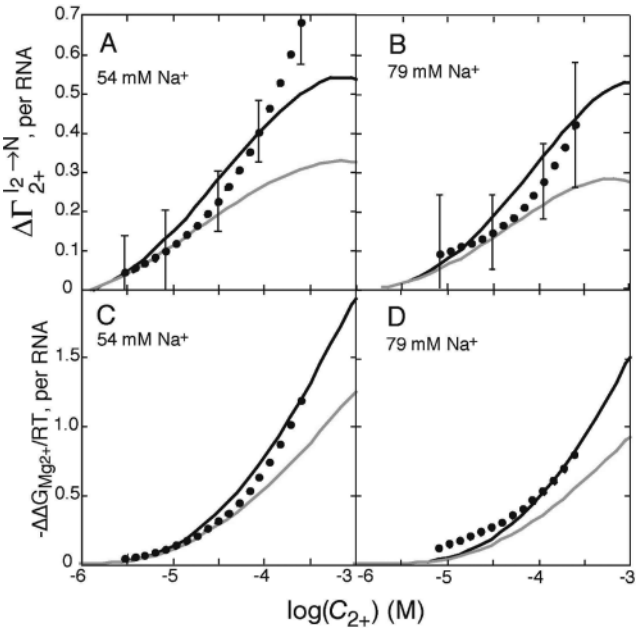

FIGURE 6: Comparison of experimental and calculated parameters related to Mg^{2+}−RNA interactions. (A and B) Plot of $\Delta C^{N}_{2+} - \Delta C^{Utail}_{2+}$ derived from the experimental data in Figure 4 (●) or $\Delta\Gamma^{I_2\rightarrow N}_{2+}$ calculated from the NLPB equation using either U-tail Near (black curve) or U-tail Far (gray curve) as a model for the I_2 state. The error bars are estimated from the errors shown in Figure 4. (C and D) Plot of the free energy of Mg^{2+}-induced RNA stabilization, $\Delta\Delta G_{Mg}{}^{2+}$, derived from the same sets of data and calculations as in panels A and B. Errors are comparable in relative size to those shown in the corresponding panels A and B. A and C refer to data and calculations obtained in buffers with 54 mM Na^+ and B and D to 79 mM Na^+.

Differences between Mg^{2+} Interactions with N and I_2 State RNAs. The differences in Γ^{RNA}_{2+} or $\Delta G_{RNA-Mg^{2+}}$ between the I_2 and N states are quantities of particular interest because they are directly related to the net stabilization of the N state relative to the I_2 state by the addition of $MgCl_2$. For these differences, systematic errors in either experiments or calculations will approximately cancel. Figure 6A and B shows the calculated quantity $\Delta\Gamma^{I_2\rightarrow N}_{2+} = \Gamma^{N}_{2+} - \Gamma^{I_2}_{2+}$ compared with the corresponding experimental quantity for the Mg^{2+}−RNA data collected at 54 and 79 mM Na^+. Calculations with the U-tail Near and Far models of the unfolded state bracket the experimental data over most of the Mg^{2+} concentration range in each case, and the differences between the two models are comparable to the experimental error in determining $\Delta\Gamma^{I_2\rightarrow N}_{2+}$. The only data that lie significantly outside of the calculated curves are $\Delta\Gamma^{I_2\rightarrow N}_{2+}$ at higher Mg^{2+} concentrations at 54 mM Na^+ (Figure 6A). Because the same experimental data are bracketed by the calculated free energy curves (Figure 6C), we do not consider the discrepancy in $\Delta\Gamma^{I_2\rightarrow N}_{2+}$ to suggest a significant departure from the Poisson−Boltzmann model of ion − RNA interactions.

The overall free energy of Mg^{2+}−RNA interactions, $\Delta G_{RNA-Mg^{2+}}$, was obtained by integration of the ΔC^{RNA}_{2+} data shown in Figure 4 for either BWYV or U-tail RNAs (eq 2) and used to find $\Delta\Delta G_{Mg^{2+}}$, the free energy of pseudoknot stabilization afforded by the addition of $MgCl_2$ (eq 4). The same quantity was also obtained from calculations with the NLPB equation. Comparisons between calculated and experimental values of $\Delta\Delta G_{Mg^{2+}}$ are shown in Figure 6C and D. As in the comparison of $\Delta\Gamma^{I_2\rightarrow N}_{2+}$ values in panels A and B of Figure 6, calculations with the U-tail Near and Far models bracket the experimental values.

Comparison of $\Delta\Gamma^{I_2\rightarrow N}_{2+}$ Obtained by Two Different Methods. $\Delta\Gamma^{I_2\rightarrow N}_{2+}$ has been measured by two different approaches in this work. One is linkage analysis (eq 6), which yielded $\Delta\Gamma^{I_2\rightarrow N}_{2+} \approx 0.73$ ions per RNA from the approximately linear dependence of unfolding free energies on ln(C_{2+}) over a Mg^{2+} concentration range spanning nearly 2 orders of magnitude (~30 μM to 2.5 mM; Figure 3B). $\Delta\Gamma^{I_2\rightarrow N}_{2+}$ was also obtained directly as the difference in excess Mg^{2+} associated with N and I_2 state RNAs; those values were smaller and strongly dependent on C_{2+}, ranging from $\Delta\Gamma^{I_2\rightarrow N}_{2+} \approx 0.22$ (C_{2+}= 30 μM) to $\Delta\Gamma^{I_2\rightarrow N}_{2+} \approx 0.68$ (C_{2+}= 0.2 mM) (Figure 6A). The two approaches appear to give inconsistent answers: linkage analysis implies that $\Delta\Gamma^{I_2\rightarrow N}_{2+}$ is constant over a wide range of C_{2+}, whereas Γ^{RNA}_{2+} measurements suggest that $\Delta\Gamma^{I_2\rightarrow N}_{2+}$ varies at least 3-fold within the same C_{2+} concentration range.

On the basis of calculations with the NLPB equation, it appears that the discrepancy between linkage analysis and Γ^{RNA}_{2+} measurements arises because linkage analysis can mask substantial variation in $\Delta\Gamma^{I_2\rightarrow N}_{2+}$. These calculations are shown in Figure 7. The calculated free energy of Mg^{2+}-induced stabilization of BWYV RNA, $\Delta\Delta G_{Mg^{2+}}$, is plotted in Figure 7A over the same range of C_{2+} used in the experimental work (30 μM to 2.5 mM). Line-fits to the plots give $\Delta\Gamma^{I_2\rightarrow N}_{2+}$ values of 0.578 or 0.265 using the U-tail Far or Near models for the I_2 state, respectively. If examined closely, deviations from linearity can be seen in the plots. If there were fewer points and a small amount of random error (as would occur in an experimental data set) these deviations would be very hard to detect. Figure 7B shows plots of $\Delta\Gamma^{I_2\rightarrow N}_{2+}$ obtained from Γ^{N}_{2+} and $\Gamma^{I_2}_{2+}$; the values of $\Delta\Gamma^{I_2\rightarrow N}_{2+}$ obtained from linkage analysis (Figure 7A) are shown as heavy horizontal bars. Clearly, the linkage analysis has averaged substantial variation in $\Delta\Gamma^{I_2\rightarrow N}_{2+}$ to make it appear as if the increase in excess Mg^{2+} associated with folding is constant over a wide range of C_{2+}. We conclude that the use of linkage analysis to obtain $\Delta\Gamma^{I_2\rightarrow N}_{2+}$ values is inherently less reliable than the direct measurement of excess Mg^{2+}, simply because very accurate data are needed to detect small degrees of curvature. Similar difficulties arise in measuring other thermodynamic quantities from first derivatives (*41*).

DISCUSSION

Experimental Measurement of Mg^{2+} Interactions with RNA. The first objective of this study was to obtain a comprehensive set of thermodynamic data on the Mg^{2+}-dependent folding of an RNA tertiary structure. Of particular interest are the Mg^{2+}−RNA interaction free energies (vertical arrows, Figure 1B), which have seldomly been measured for any RNA. A particular reason for choosing BWYV RNA for this study was the accessibility of $\Delta G_{N-Mg^{2+}}$ to direct measurement. The stability of the native RNA in relatively low concentrations of monovalent salt allowed Mg^{2+} interactions with the folded RNA to be experimentally and

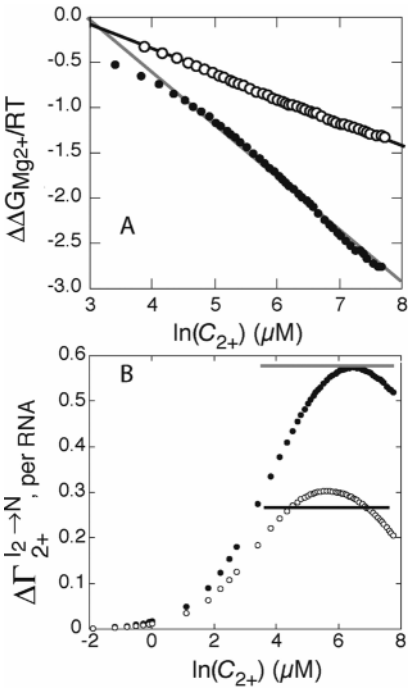

FIGURE 7: Relationship of $\Delta\Gamma^{I_2\rightarrow N}_{2+}$ calculated either from the linkage analysis of electrostatic free energies (eq 5) or from the changes in excess Mg^{2+} ions per RNA associated with BWYV tertiary structure folding, $\Gamma^{N}_{2+} - \Delta\Gamma^{I_2}_{2+}$. Free energies and Γ^{RNA}_{2+} values were calculated from the NLPB equation specifying a bulk monovalent cation concentration of 54 mM. (A) Free energy of Mg^{2+}-induced stabilization of the folded state ($\Delta\Delta G_{Mg^{2+}}$) calculated from the NLPB equation using U-tail Near (●) or U-tail Far (○) as a model for the unfolded state (I_2). Slopes of the lines through the data points were used to calculate values of $\Delta\Gamma^{I_2\rightarrow N}_{2+}$ from the linkage analysis (eq 3) of 0.578 and 0.265, respectively. (B) $\Delta\Gamma^{I_2\rightarrow N}_{2+}$ directly calculated from Γ^{N}_{2+} and $\Delta\Gamma^{I_2}_{2+}$ for U-tail Near (●) or U-tail Far (○). Horizontal lines are drawn for the $\Delta\Gamma^{I_2\rightarrow N}_{2+}$ values found in panel A; their end points correspond to the range of ln(C_{2+}) used in the calculation.

theoretically determined without complications from Mg^{2+}-induced conformational transitions. Though some transfer RNAs have similarly stable tertiary structures in the absence of Mg^{2+} (*5*, *42*), most RNA tertiary structures require some Mg^{2+} or very high monovalent salt concentrations to fold (*43*).

The critical experimental data from this study are the dependence of ΔC^{RNA}_{2+} on the bulk Mg^{2+} concentration (C_{2+}) for two RNAs, the folded BWYV pseudoknot (N) and a mimic of the partially unfolded pseudoknot (U-tail) (Figure 4). Some aspects of the magnitudes of the excess Mg^{2+}−RNA curves are noteworthy. Both ΔC^{N}_{2+} and ΔC^{Utail}_{2+} increase monotonically with increasing C_{2+}, but accumulation of Mg^{2+} neutralizes only a small fraction of the phosphate charge in the accessible range of C_{2+}. For this RNA, accumulation of Na^+ and/or exclusion of Cl^- play the primary role in the neutralization of the phosphate charges even at high Mg^{2+} concentrations. At low C_{2+}, ΔC^{N}_{2+} asymptotically approaches zero. Thus, there is no evidence of strong, stoichiometric Mg^{2+} ion binding by the folded RNA, which would appear as the persistence of one or more excess ions per RNA (at least 0.036 ions per nucleotide) at low C_{2+}. Finally, all ΔC^{RNA}_{2+} values decrease when the Na^+ concentration increases from 54 to 79 mM. This behavior is expected, regardless of the modes by which Mg^{2+} ions interact with the RNA, because of the strong thermodynamic coupling between all ions interacting with an RNA (*28*).

Measurements of $\Delta\Gamma^{I_2\rightarrow N}_{2+}$. The calculations presented in Figure 7 highlight the difficulty in measuring $\Delta\Gamma^{I_2\rightarrow N}_{2+}$ from the dependence of the RNA-folding free energy on Mg^{2+} concentration. Because the extent of RNA folding (and thus $\Delta G°_{obs,Mg^{2+}}$) is readily measured by any of several methods, linkage analysis and related methods have been the preferred approaches for obtaining $\Delta\Gamma^{I_2\rightarrow N}_{2+}$ in most RNA-folding studies. Usually, the Hill equation is used to fit folding data, and the Hill exponent n is reported in place of $\Delta\Gamma^{I_2\rightarrow N}_{2+}$ (*44*, *45*). (The Hill equation is related to linkage analysis, with the assumption that the reaction under consideration is described by a stoichiometric binding equilibrium with n as the number of ligands taken up in the reaction (*34*).) The success of the Hill equation in fitting RNA-folding data has been used to support the idea that n is a constant measuring the number of ions binding to specific sites in the folded RNA (*46*, *47*). But as suggested by Figure 7, n (or $\Delta\Gamma^{I_2\rightarrow N}_{2+}$) may be much more variable than apparent from the fits of unfolding data to the Hill equation. Caution is, therefore, needed in using $\Delta\Gamma^{I_2\rightarrow N}_{2+}$ from linkage analysis to devise models for Mg^{2+}-dependent RNA folding.

The alternative approach for finding $\Delta\Gamma^{I_2\rightarrow N}_{2+}$, from measurements of ΔC^{N}_{2+} and ΔC^{Utail}_{2+}, relies on the assumption that U-tail RNA accurately mimics the partially unfolded state. Because calculations with U-tail Near and U-tail Far RNAs suggest that changes in the ensemble of I_2 conformations will affect $\Gamma^{I_2}_{2+}$, it is conceivable that different stacking or mispairing interactions in U-tail RNA versus BWYV RNA in the I_2 state could cause the two RNAs to interact differently with Mg^{2+}. This does not appear to be a serious problem. $\Delta\Gamma^{I_2\rightarrow N}_{2+}$ calculated from measurements made on BWYV and U-tail RNAs at 0.2 mM Mg^{2+} is 0.68 ions/RNA, which compares well with the value of 0.73 ions/RNA calculated from linkage analysis when the midpoint of the Mg^{2+} concentration range used is $C_{2+} = 0.2$ mM.

Calculations Using the NLPB Equation. An objective of this study was to compare experimental measurements of Mg^{2+} accumulation by RNA to calculations based on the Poisson−Boltzmann model of ion interactions. At the Na^+ and RNA concentrations used in the experiments reported here, the excess Mg^{2+} ions per RNA, ΔC^{RNA}_{2+}, closely approximates the thermodynamic quantity Γ^{RNA}_{2+} (*33*). Both Γ^{RNA}_{2+} and the electrostatic free energy of Mg^{2+}−RNA interactions can be directly calculated from theory (*24*, *36*). In this work, we have used the nonlinear Poisson−Boltzmann (NLPB) equation to estimate the energetic contributions of Mg^{2+} to the folding of the BWYV RNA. The use of this equation to derive ion distributions and electrostatic free energies relevant to macromolecules in ionic solutions has been extensively discussed (*10*, *31*, *36*, *48*). Poisson−Boltzmann theory assumes that the ions surrounding the RNA are distributed according to the Boltzmann distribution law governed only by the mean electrostatic potential. As a result of the strong negative electrostatic potentials around the RNA, cations accumulate in the vicinity of the RNA surface, whereas anions are pushed out of this region. These surrounding ions have been referred to as diffuse ions (*6*).

However, in its simplest form as used here, PB theory does not account for ion size, changes in hydration, or interion correlations. Therefore, simple NLPB models cannot be used to describe "chelated" ions for which partial dehydration and van der Waals contacts may be important energetic factors in their interactions with RNA (*6*, *31*, *32*, *49*). In addition, comparisons of Monte Carlo simulations of explicit Mg^{2+} and Na^+ ions near DNA with NLPB-based calculations of DNA−ion interactions suggest that the neglect of ion size in Poisson−Boltzmann theory causes the calculations to underestimate Γ_{2+} (*31*). The magnitude of the underestimation is comparable to the discrepancy between NLPB-based calculations and experimentally measured excess Mg^{2+} seen with BWYV RNA (Figure 4) and double stranded RNA (*31*, *32*, *49*).

Nevertheless, even simple calculations based on the NLPB equation have provided significant quantitative insights into the free energy of Mg^{2+} interactions with helical DNA and RNA (*31*) and folded tRNA (*10*). The success of this theory arises from its ability to fully account for the long-range electrostatic interactions among all charged bodies in solution. At this scale, local effects due to ion size, changes in hydration, and interion correlations are often not significant. The NLPB equation has been particularly useful for calculating differences in electrostatic free energies between two states of a nucleic acid (e.g., p*K* shifts in bound ligands (*48*, *50*) and salt dependence of ligand binding (*51*, *52*)), in which case the systematic errors in the calculations tend to cancel.

Indeed, we find that the NLPB model provides a reasonable estimate of $\Delta G_{RNA-Mg^{2+}}$: the experimental data are nearly all bracketed by the calculated values of $\Delta\Gamma_{2+}^{I_2\rightarrow N}$ and $\Delta\Delta G_{Mg^{2+}}$ values obtained with the Near and Far models of U-tail RNA (Figure 6). These data are consistent with the idea that Mg^{2+}-induced stabilization of BWYV RNA is entirely a consequence of favorable changes in the free energy of diffuse ion interactions upon folding of the RNA. A similar conclusion about the dominant role of diffuse ions was reached for the folding of $tRNA^{phe}$ tertiary structure, on the basis of a comparison of NLPB-based calculations with available data on the accumulation of excess Mg^{2+} by folded and partially denatured tRNA (*8*, *10*). These studies show that diffuse Mg^{2+} ion interactions provide a substantial free energy favoring the formation of RNA tertiary structures, purely as a consequence of the more negative electostatic potential of a compactly folded RNA.

In addition to the stabilization afforded by diffuse Mg^{2+} ions, folded RNAs may also derive favorable free energy from direct contacts with Mg^{2+} ions. In the case of a ribosomal RNA fragment, which chelates a Mg^{2+} ion in a pocket of unusually high electrostatic potential, it was found that the free energy of binding the single chelated ion could contribute a large fraction of the overall free energy of Mg^{2+} interactions with the folded RNA (*12*). A separate estimate of the free energy of ion chelation by the RNA, taking into account changes in ion and RNA hydration energies, was necessary to obtain good agreement of the calculations with experimental data (*8*). Because a crystal structure of the BWYV pseudoknot shows $Mg(H_2O)_7^{2+}$ located at a specific position in the G−C-rich major groove of Helix 1 (*14*), it might be asked whether the positioning of Mg^{2+} at this location provides additional folding free energy, similar to the chelated ion in the rRNA fragment just mentioned. We do not attach any special thermodynamic significance to this crystallographically observed ion for several reasons. First, the most negative electrostatic potential of an RNA helix is in the major groove, which, therefore, should accumulate Mg^{2+} ions simply on the basis of Coulombic attraction (*12*, *53*). At liquid nitrogen temperatures used for crystallography, ions in the groove may occupy distinct positions. Second, strong interactions of an ion at a specific site within the RNA would cause Γ_{2+}^{N} or $\Delta\Gamma_{2+}^{I_2\rightarrow N}$ to have minimum values of 1 ion/RNA (0.036 ion/nucleotide) at low C_{2+}. This is clearly not the case (Figures 4 and 6). Third, the NLPB-based calculations should underestimate $\Delta\Gamma_{2+}^{I_2\rightarrow N}$ (by 1 ion/RNA) and $-\Delta\Delta G_{Mg^{2+}}$ at low C_{2+}. Again, the calculations do not show any such discrepancy.

Importance of the I State for Models of RNA Folding. The details of the RNA's 3D geometry and charge distribution are crucial to the calculation. Thus, it was important to determine the protonation state of C8 in the folded structure; if C8 were unprotonated, the Γ_{2+}^{RNA} values would have been significantly higher. The more critical problem is the structure in the I_2 state; it is unreasonable to think that the flexible, single-stranded portion of the partially unfolded RNA can be represented by a discrete structural model. We circumvented this problem by constructing two extreme models (U-tail Near and U-tail Far) that are meant to bracket the likely distribution of the single-strand conformations. Because the electrostatic free energies are determined by long-range interactions that depend mostly on RNA charge density, this approach has proved adequate for asking whether BWYV RNA-folding energetics are dominated by diffuse ion interactions or whether other modes of ion interactions must be included.

The I state model used in calculations can result in 50% differences in the critical quantities $\Delta\Gamma_{2+}^{I_2\rightarrow N}$ and $\Delta\Delta G_{Mg^{2+}}$ (Figure 6). Thus, the accuracy of I state models could limit the ability of theoretical models to distinguish subtle differences in ways ions interact with RNA. Just as models of the unfolded state of proteins have become essential to discussions of the protein folding problem (*54*), models of the I state of an RNA will be an important component of any comprehensive theory of RNA folding.

ACKNOWLEDGMENT

We thank Mr. Kingsley Onunogbo for highly purified T7 RNA polymerase.

REFERENCES

1. Ferre-D'Amare, A. R., and Doudna, J. A. (1999) RNA folds: insights from recent crystal structures, *Annu. Rev. Biophys. Biomol. Struct. 28*, 57−73.
2. Moore, P. B. (1999) Structural motifs in RNA, *Annu. Rev. Biochem. 68*, 287−300.
3. Zhuang, X., and Rief, M. (2003) Single-molecule folding, *Curr. Opin. Struct. Biol. 13*, 88−97.
4. Caprara, M. G., and Nilsen, T. W. (2000) RNA: versatility in form and function, *Nat. Struct. Biol. 7*, 831−833.
5. Cole, P. E., Yang, S. K., and Crothers, D. M. (1972) Conformational changes of transfer ribonucleic acid. Equilibrium phase diagrams, *Biochemistry 11*, 4358−4368.

6. Draper, D. E., Grilley, D., and Soto, A. M. (2005) Ions and RNA folding, *Annu. Rev. Biophys. Biomol. Struct. 34*, 221−243.
7. Stein, A., and Crothers, D. M. (1976) Conformational changes of transfer RNA. The role of magnesium(II), *Biochemistry 15*, 160−167.
8. Misra, V. K., and Draper, D. E. (2002) The linkage between magnesium binding and RNA folding, *J. Mol. Biol. 317*, 507−521.
9. Schimmel, P. R., and Redfield, A. G. (1980) Transfer RNA in solution: selected topics, *Ann. Rev. Biophys. Bioeng. 9*, 181−221.
10. Misra, V. K., and Draper, D. E. (2000) Mg(2+) binding to tRNA revisited: the nonlinear Poisson-Boltzmann model, *J. Mol. Biol. 299*, 813−825.
11. Draper, D. E. (2004) A guide to ions and RNA structure, *RNA 10*, 335−343.
12. Misra, V. K., and Draper, D. E. (2001) A thermodynamic framework for Mg2+ binding to RNA, *Proc. Natl. Acad. Sci. U.S.A. 98*, 12456−12461.
13. Su, L., Chen, L., Egli, M., Berger, J. M., and Rich, A. (1999) Minor groove RNA triplex in the crystal structure of a ribosomal frameshifting viral pseudoknot, *Nat. Struct. Biol. 6*, 285−292.
14. Egli, M., Minasov, G., Su, L., and Rich, A. (2002) Metal ions and flexibility in a viral RNA pseudoknot at atomic resolution, *Proc. Natl. Acad. Sci. U.S.A. 99*, 4302−4307.
15. Puglisi, J. D., and Wyatt, J. R. (1995) Biochemical and NMR studies of RNA conformation with an emphasis on RNA pseudoknots, *Methods Enzymol. 261*, 323−350.
16. He, B., Rong, M., Lyakhov, D., Gartenstein, H., Diaz, G., Castagna, R., McAllister, W. T., and Durbin, R. K. (1997) Rapid mutagenesis and purification of phage RNA polymerases, *Protein Expression Purif. 9*, 142−151.
17. Cantor, C. R., Warshaw, M. M., and Shapiro, H. (1970) Oligonucleotide interactions. 3. Circular dichroism studies of the conformation of deoxyoligonucleotides, *Biopolymers 9*, 1059−1077.
18. Marky, L. A., Blumenfeld, K. S., Kozlowski, S., and Breslauer, K. J. (1983) Salt-dependent conformational transitions in the self-complementary deoxydodecanucleotide d(CGCAATTCGCG): evidence for hairpin formation, *Biopolymers 22*, 1247−1257.
19. Grilley, D., Soto, A. M., and Draper, D. E. (2006) Direct quantitation of Mg2+: RNA interactions by use of a fluorescent dye, *Methods Enzymol.*, in press.
20. Draper, D. E., Bukhman, Y. V., and Gluick, T. C. (2000) Thermal Methods for the Analysis of RNA Folding Pathways, in *Current Protocols in Nucleic Acid Chemistry* (Beaucage, S. L., Bergstrom, D. E., Glick, G. D., and Jones, R. A., Eds.) section 11.3, John Wiley & Sons, New York.
21. Grilley, D., Soto, A. M., and Draper, D. E. (2006) Mg2+-RNA interaction free energies and their relationship to the folding of RNA tertiary structures, *Proc. Natl. Acad. Sci. U.S.A. 103*, 14003−14008.
22. Record, M. T., Jr., Anderson, C. F., and Lohman, T. M. (1978) Thermodynamic analysis of ion effects on the binding and conformational equilibria of proteins and nucleic acids: the roles of ion association or release, screening, and ion effects on water activity, *Q. Rev. Biophys. 11*, 103−178.
23. Sharp, K. A. (1995) Polyelectrolyte electrostatics: Salt dependence, entropic, and enthalpic contributions to free energy in the nonlinear Poisson-Boltzmann model, *Biopolymers 36*, 227−243.
24. Chen, S. W., and Honig, B. (1997) Monovalent and divalent salt effects on electrostatic free energies defined by the nonlinear Poisson-Boltzmann equation: Application to DNA binding reactions, *J. Phys. Chem. B. 101*, 9113−9118.
25. Weiner, S. J., Kollman, P. A., Case, D. A., Singh, U. C., Ghio, C., Alagona, G., Profeta, S., Jr., and Weiner, P. (1984) A new force field for molecular mechanical simulation of nucleic acids and proteins, *J. Am. Chem. Soc. 106*, 765−784.
26. Petrov, A. S., Lamm, G., and Pack, G. R. (2004) The triplex-hairpin transition in cytosine-rich DNA, *Biophys. J. 87*, 3954−3973.
27. Misra, V. K., Sharp, K. A., Friedman, R. A., and Honig, B. (1994) Salt effects on ligand-DNA binding: Minor groove binding antibiotics, *J. Mol. Biol. 238*, 245−263.
28. Misra, V. K., Shiman, R., and Draper, D. E. (2003) A thermodynamic framework for the magnesium-dependent folding of RNA, *Biopolymers 69*, 118−136.
29. Nixon, P. L., and Giedroc, D. P. (2000) Energetics of a strongly pH dependent RNA tertiary structure in a frameshifting pseudoknot, *J. Mol. Biol. 296*, 659−671.
30. Anderson, C. F., Felitsky, D. J., Hong, J., and Record, M. T. (2002) Generalized derivation of an exact relationship linking different coefficients that characterize thermodynamic effects of preferential interactions, *Biophys. Chem. 102*, 497−511.
31. Misra, V. K., and Draper, D. E. (1999) The interpretation of Mg^{2+} binding isotherms for nucleic acids using Poisson-Boltzmann theory, *J. Mol. Biol. 294*, 1135−1147.
32. Ni, H., Anderson, C. F., and Record, M. T., Jr. (1999) Quantifying the thermodynamic consequences of cation (M2+, M+) accumulation and anion (X-) exclusion in mixed salt solutions of polyanionic DNA using Monte Carlo and Poisson-Boltzmann calculations of ion-polyion preferential interaction coefficients, *J. Phys. Chem. B 103*, 3489−3504.
33. Anderson, C. F., and Record, M. T., Jr. (1993) Salt dependence of oligoion-polyion binding: A thermodynamic description based on preferential interaction coefficients, *J. Phys. Chem. 97*, 7116−7126.
34. Wyman, J., Jr. (1964) Linked functions and reciprocal effects in hemoglobin: A second look, *Adv. Protein Chem. 19*, 223−286.
35. Moody, E. M., Lecomte, J. T., and Bevilacqua, P. C. (2005) Linkage between proton binding and folding in RNA: A thermodynamic framework and its experimental application for investigating pKa shifting, *RNA 11*, 157−172.
36. Sharp, K. A., and Honig, B. (1990) Calculating total electrostatic energies with the nonlinear Poisson-Boltzmann equation, *J. Phys. Chem. 94*, 7684−7692.
37. Eisenberg, H., and Felsenfeld, G. (1967) Studies of the temperature-dependent conformation and phase separation of polyriboadenylic acid solutions at neutral pH, *J. Mol. Biol. 30*, 17−37.
38. Inners, L. D., and Felsenfeld, G. (1970) Conformation of polyribouridylic acid in solution, *J. Mol. Biol. 50*, 373−389.
39. Murphy, M. C., Rasnik, I., Cheng, W., Lohman, T. M., and Ha, T. (2004) Probing single-stranded DNA conformational flexibility using fluorescence spectroscopy, *Biophys. J. 86*, 2530−2537.
40. Record, M. T., Jr., Zhang, W., and Anderson, C. F. (1998) Analysis of effects of salts and uncharged solutes on protein and nucleic acid equilibria and processes: A practical guide to recognizing and interpreting polyelectrolyte effects, Hofmeister effects, and osmotic effects of salts, *Adv. Protein Chem. 51*, 281−353.
41. Chaires, J. B. (1997) Possible origin of differences between van't Hoff and calorimetric enthalpy estimates, *Biophys. Chem. 64*, 15−23.
42. Römer, R., and Hach, R. (1975) tRNA conformation and magnesium binding. A study of a yeast phenylalanine-specific tRNA by a fluorescent indicator and differential melting curves, *Eur. J. Biochem. 55*, 271−284.
43. Bukhman, Y. V., and Draper, D. E. (1997) Affinities and selectivities of divalent cation binding sites within an RNA tertiary structure, *J. Mol. Biol. 274*, 1020−1031.
44. Lynch, D. C., and Schimmel, P. R. (1974) Cooperative binding of magnesium to transfer ribonucleic acid studied by a fluorescent probe, *Biochemistry 13*, 1841−1852.
45. Silverman, S. K., and Cech, T. R. (1999) Energetics and cooperativity of tertiary hydrogen bonds in RNA structure, *Biochemistry 38*, 8691−8702.
46. Fang, X., Pan, T., and Sosnick, T. R. (1999) A thermodynamic framework and cooperativity in the tertiary folding of a Mg2+-dependent ribozyme, *Biochemistry 38*, 16840−16846.
47. Das, R., Travers, K. J., Bai, Y., and Herschlag, D. (2005) Determining the Mg stoichiometry for folding an RNA metal ion core, *J. Am. Chem. Soc. 127*, 8272−8273.
48. Misra, V. K., and Honig, B. (1995) On the magnitude of the electrostatic contribution to ligand-DNA interactions, *Proc. Natl. Acad. Sci. U.S.A. 92*, 4691−4695.
49. Tan, Z. J., and Chen, S. J. (2005) Electrostatic correlations and fluctuations for ion binding to a finite length polyelectrolyte, *J. Chem. Phys. 122*, 44903.
50. Misra, V. K., Hecht, J. L., Yang, A. S., and Honig, B. (1998) Electrostatic contributions to the binding free energy of the lambda cI repressor to DNA, *Biophys. J. 75*, 2262−2273.
51. Misra, V. K., Hecht, J. L., Sharp, K. A., Friedman, R. A., and Honig, B. (1994) Salt effects on protein-DNA interactions. The λcI repressor and *Eco*RI endonuclease, *J. Mol. Biol. 238*, 264−280.
52. García-García, C., and Draper, D. E. (2003) Electrostatic interactions in a peptide-RNA complex, *J. Mol. Biol. 331*, 75−88.

53. Chin, K., Sharp, K. A., Honig, B., and Pyle, A. M. (1999) Calculating the electrostatic properties of RNA provides new insights into molecular interactions and function, *Nat. Struct. Biol. 6*, 1055−1061.

54. Rose, G. D. (2002) Getting to know u, *Adv. Protein Chem. 62*, xv−xxi.

BI0616753